EUROPEAN SYNCHROTRON RADIATION FACILITY

INSTALLATION EUROPEENNE DE RAYONNEMENT SYNCHROTRON

Experiment Report Form

The double page inside this form is to be filled in by all users or groups of users who have had access to beam time for measurements at the ESRF.

Once completed, the report should be submitted electronically to the User Office via the User Portal:
https://wwws.esrf.fr/misapps/SMISWebClient/protected/welcome.do

Deadlines for submission of Experimental Reports

Experimental reports must be submitted within the period of 3 months after the end of the experiment.

Experiment Report supporting a new proposal ("relevant report")

If you are submitting a proposal for a new project, or to continue a project for which you have previously been allocated beam time, you must submit a report on each of your previous measurement(s):

- even on those carried out close to the proposal submission deadline (it can be a *"preliminary report"),*
- even for experiments whose scientific area is different form the scientific area of the new proposal,
- carried out on CRG beamlines.

You must then register the report(s) as "relevant report(s)" in the new application form for beam time.

Deadlines for submitting a report supporting a new proposal

- 1st March Proposal Round - **5th March**
- 10th September Proposal Round - **13th September**

The Review Committees reserve the right to reject new proposals from groups who have not reported on the use of beam time allocated previously.

Reports on experiments relating to long term projects

Proposers awarded beam time for a long term project are required to submit an interim report at the end of each year, irrespective of the number of shifts of beam time they have used.

Published papers

All users must give proper credit to ESRF staff members and proper mention to ESRF facilities which were essential for the results described in any ensuing publication. Further, they are obliged to send to the Joint ESRF/ ILL library the complete reference and the abstract of all papers appearing in print, and resulting from the use of the ESRF.

Should you wish to make more general comments on the experiment, please note them on the User Evaluation Form, and send both the Report and the Evaluation Form to the User Office.

Instructions for preparing your Report

- fill in a separate form for each project or series of measurements.
- type your report in English.
- include the experiment number to which the report refers.
- make sure that the text, tables and figures fit into the space available.
- if your work is published or is in press, you may prefer to paste in the abstract, and add full reference details. If the abstract is in a language other than English, please include an English translation.

ESRF	**Experiment title:** Revealing 3D nanostructure for improved biophysical MRI models in brain diseases	**Experiment number**: LS 2840
Beamline: ID16A-NI	**Date of experiment**: from: 28/11 2018 to: 3/12 2018	**Date of report**:
Shifts: 15	**Local contact(s)**: Alexandra Pacureanu	*Received at ESRF:*

Names and affiliations of applicants (* indicates experimentalists):

Mariam Andersson*, DTU, Denmark

Tim Dyrby*, DTU, Denmark

Martin Bech*, Lund University, Sweden

Alessandro Daducci, University of Verona, Italy

Anders Dahl, DTU, Denmark

Alexandra Joita Pacureanu*, ESRF, France

Report:

The experiment was conducted in accordance with the proposal.

Results are published in the Proceedings of the National Academy of Sciences.

Andersson M, Kjer HM, Rafael-Patino J, Pacureanu A, Pakkenberg B, Thiran JP, Ptito M, Bech M, Dahl AB, Dahl VA, Dyrby TB. Axon morphology is modulated by the local environment and impacts the noninvasive investigation of its structure–function relationship. Proceedings of the National Academy of Sciences. 2020 Dec 29;117(52):33649-59.

Extract from publication:

Abstract

Axonal conduction velocity, which ensures efficient function of the brain network, is related to axon diameter. Noninvasive, in vivo axon diameter estimates can be made with diffusion magnetic resonance imaging, but the technique requires three-dimensional (3D) validation. Here, high-resolution, 3D synchrotron X-ray nano-holotomography images of white matter samples from the corpus callosum of a monkey brain reveal that blood vessels, cells, and vacuoles affect axonal diameter and trajectory. Within single axons, we find that the variation in diameter and conduction velocity correlates with the mean diameter, contesting the value of precise diameter determination in larger axons. These complex 3D axon morphologies drive previously reported 2D trends in axon diameter and *g*-ratio. Furthermore, we find that these morphologies bias the estimates of axon diameter with diffusion magnetic resonance imaging and, ultimately, impact the investigation and formulation of the axon structure–function relationship.

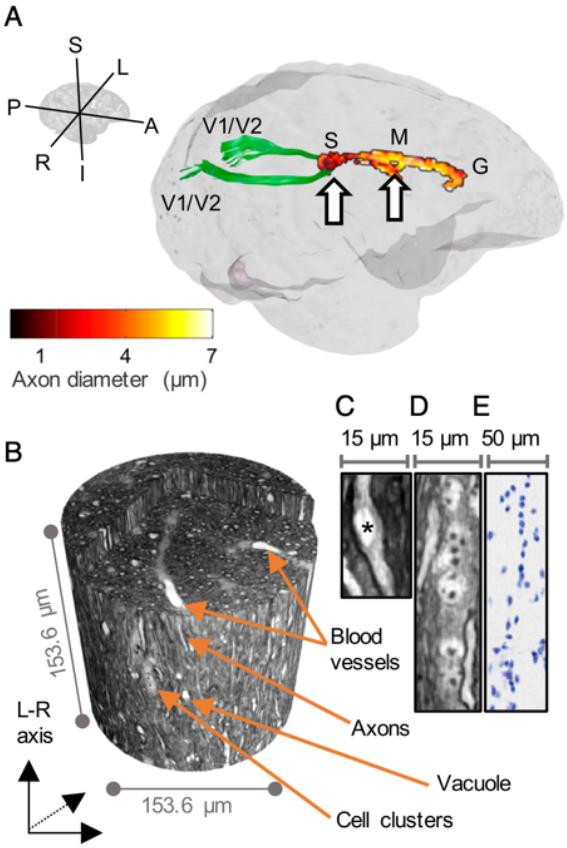

Fig 1. Observed anatomical microstructures within the white matter of the monkey brain. (A) Diffusion-MRI mean AD estimations with the ActiveAx method in the midsagittal plane of corpus callosum (CC) of the monkey brain spanning the splenium (S), midbody (M), and genu (G). The arrows show biopsy locations. The interhemispheric callosal connection between primary visual cortices (V1/V2) is delineated with tractography and is shown in green. (B) Three-dimensional XNH volume from the splenium with an isotropic voxel size of 75 nm, showing detectable anatomical features. The volume interior is exposed to reveal the vessels. (C) Close-up of a vacuole (asterisk). (D) Close-up of a cell cluster. (E) Nissl stain light microscopy image showing nuclei in the same splenium region as D in an age-matched monkey (BrainMaps: An Interactive Multiresolution Brain Atlas; brainmaps.org).

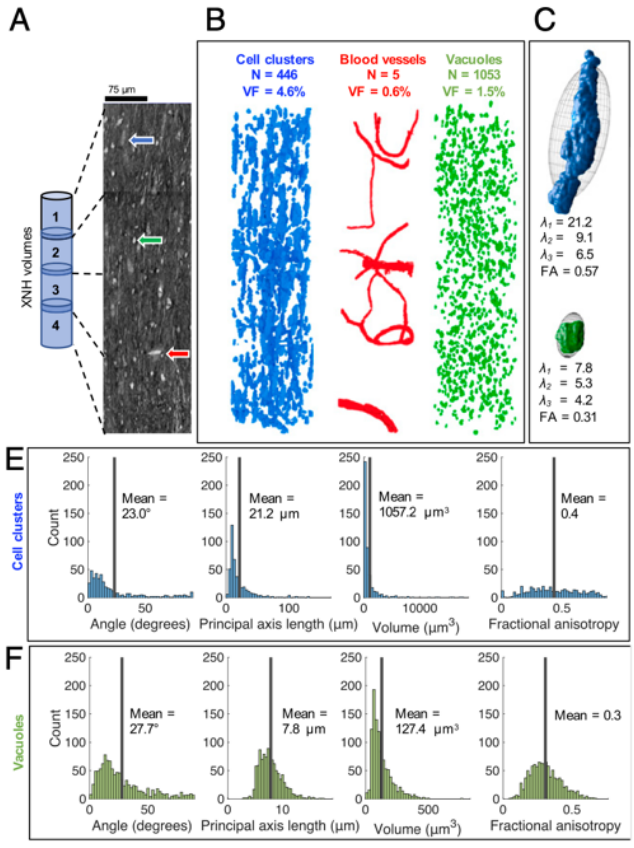

Fig. 2. Volumetric quantification of cell clusters, vessels, and vacuoles. (A) Two-dimensional slice through four overlapping XNH volumes (13.6-μm overlap) of the monkey brain splenium. Blue arrow, cell body. Green arrow, vacuole. Red arrow, blood vessel. (B) Three-dimensional reconstructions of the cell clusters (blue), blood vessels (red), and vacuoles (green) within the cylindrical volume of length 584.4 μm and diameter 153.6 μm. (C) $\lambda 1$, $\lambda 2$, and $\lambda 3$ denote the average first, second, and third principal-component lengths of tensors fitted to the cell cluster/vacuole structures. These are visualized by ellipsoids. In blue/green: examples of an individual cell cluster/vacuole. (D) Three-dimensional visualization of cell cluster, blood vessel, and vacuole segmentations. (E and F) Histo- grams showing the mean values and distributions of the following: inclination angle (compared to the axon population direction), principal axis length, mean volume, and FA across the cellular (blue) and vacuole (green) components, respectively.

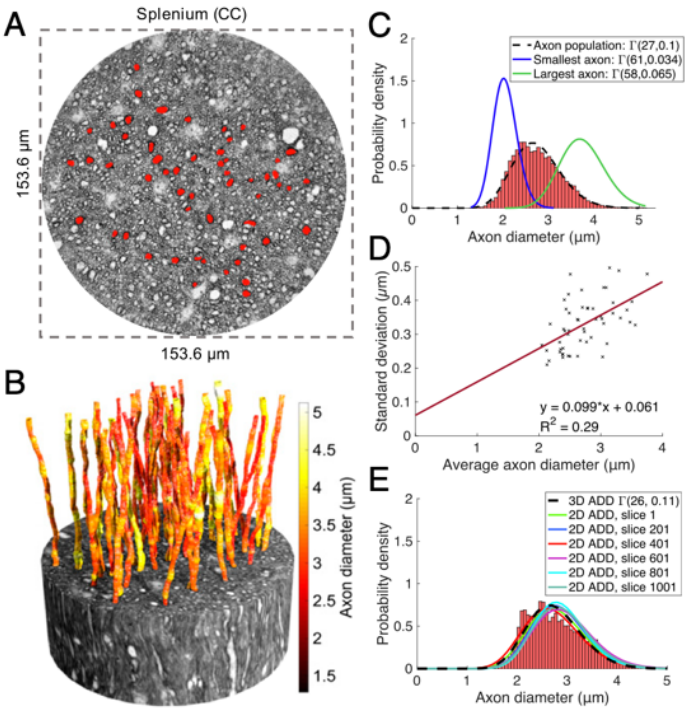

Fig 3. Distribution and morphology of large axons. (A) Distribution of 54 large axons (red) in a 2D slice of the monkey splenium. (B) Fifty-four seg- mented axons from the monkey splenium. The axon lengths range from 124 to 170 µm, with average ADs between 2.1 and 3.8 µm. (C) Combined 3D ADD consisting of diameter measurements every 150 nm along all 54 axons and associated gamma distribution fit (black). For comparison, the fits of the longitudinal ADDs of the thinnest (blue) and thickest axon (green) are shown. (D) The SD of the longitudinal AD correlates positively with average AD. (E) Histogram and gamma distribution fit (black striped line) of com- bined 3D ADD, along with gamma distribution fits of the 2D ADD, sampled every 200 slices of the image subvolume in which all 54 axons were present.

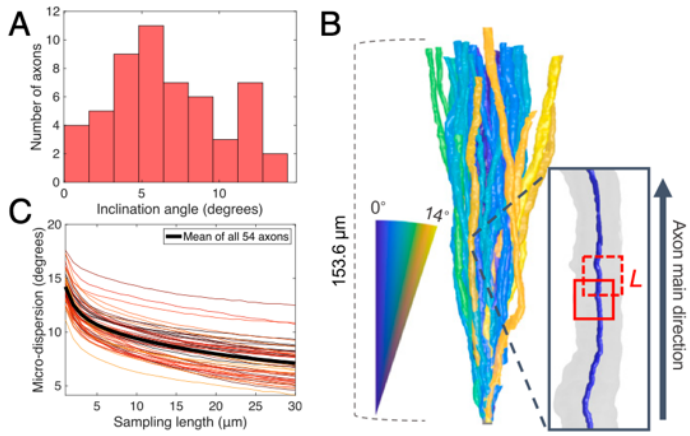

Fig 4. Trajectory variations of large axons. (A) Histogram of the OD—the axonal inclination with respect to the main bundle direction—within the axon population. (B) Fifty-four axons from the splenium of the monkey brain translated to a common origin to illustrate the mesoscopic dispersion within the volume. Axon color represents inclination angle compared to the z axis. The Inset shows the quantification of microdispersion along axons: The axon is aligned with the z axis and a window of length L slides along the axon centerline (blue) at intervals of L/4. A principal-component analysis is performed on points within the window to determine their directionality. The inclination angle to the z axis is calculated and averaged over all windows. (C) Variation of microdispersion relative to main axon direction with sampling length, L (data points every 1 µm).

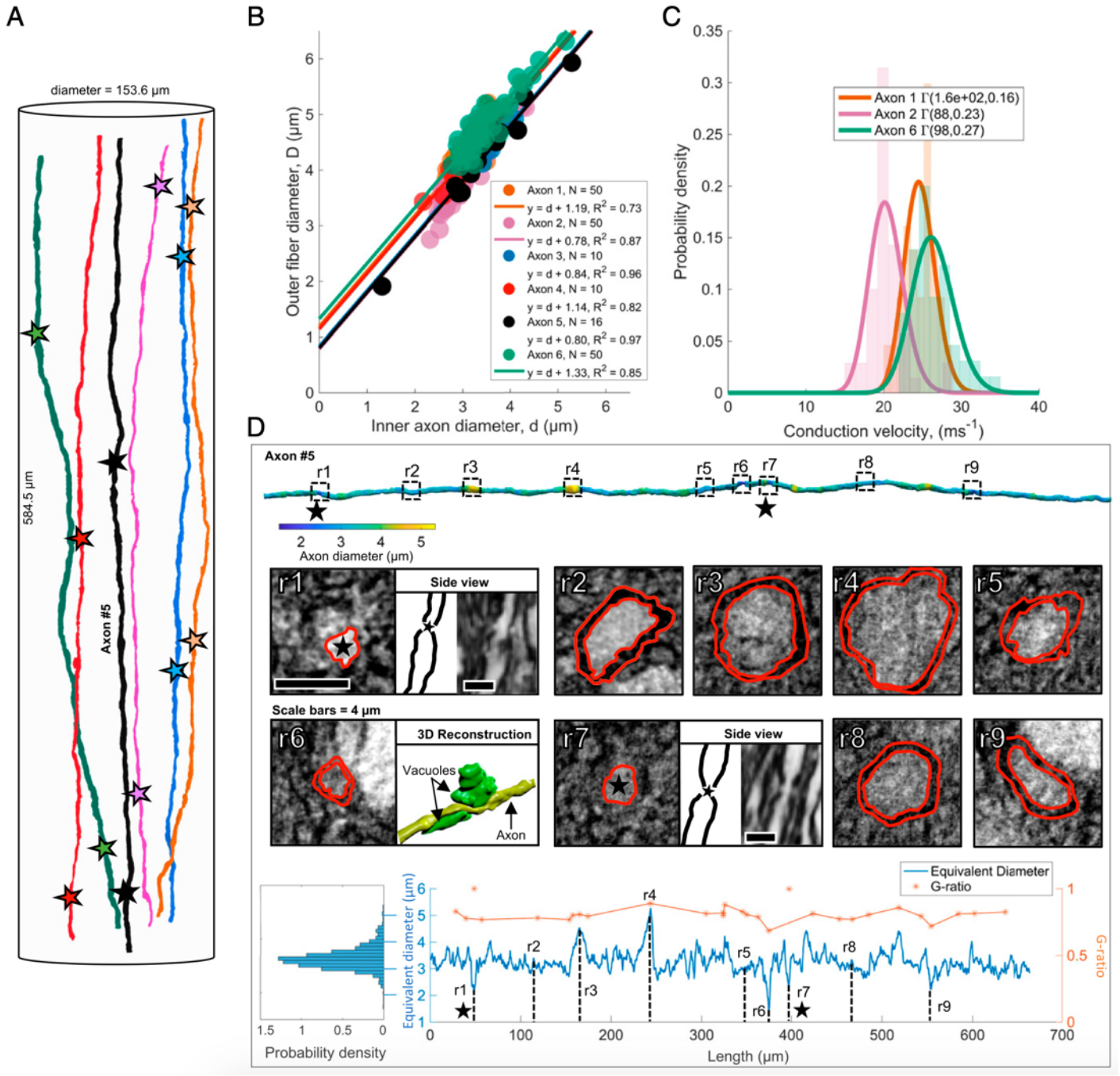

Fig 5. Long-range quantification of axon morphology and myelination. (A) Six long axons segmented from the extended cylindrical XNH volume of the monkey splenium shown in Fig. 2 A and D. The stars mark identified nodes of Ranvier. (B) Inner AD vs. outer fiber diameter (including myelin sheath) at N randomly sampled points along the internodes of the six axons. Straight lines represent linear fits to the six datasets. The high linear correlation suggests that the myelin thickness remains approximately constant along the internodes, and that the y intercept is representative of twice the myelin thickness. (C) Histograms and associated gamma distribution fits of CVs along the internodes of axons 1, 2, and 6. (D) Row 1: segmentation of long axon (number 5, black, in A and B), colored according to diameter. The dotted squares marked r1–r9 indicate nine ROIs. Black stars mark the positions of the nodes of Ranvier. Row 2: ROI intensity images. The red lines show a manual segmentation of the inner axonal boundary and the outer myelin boundary, respectively. At r1 and r7, nodes of Ranvier are shown in an orthogonal view. At r6, the axon (yellow) is squeezed by two vacuoles (green). Row 3: on Left: ADD along axon. Blue line: the longitudinal equivalent AD measured every 150 nm along the axonal trajectory. In orange, the g-ratio for the 9 marked ROIs and 20 additional randomly generated positions along the axon.

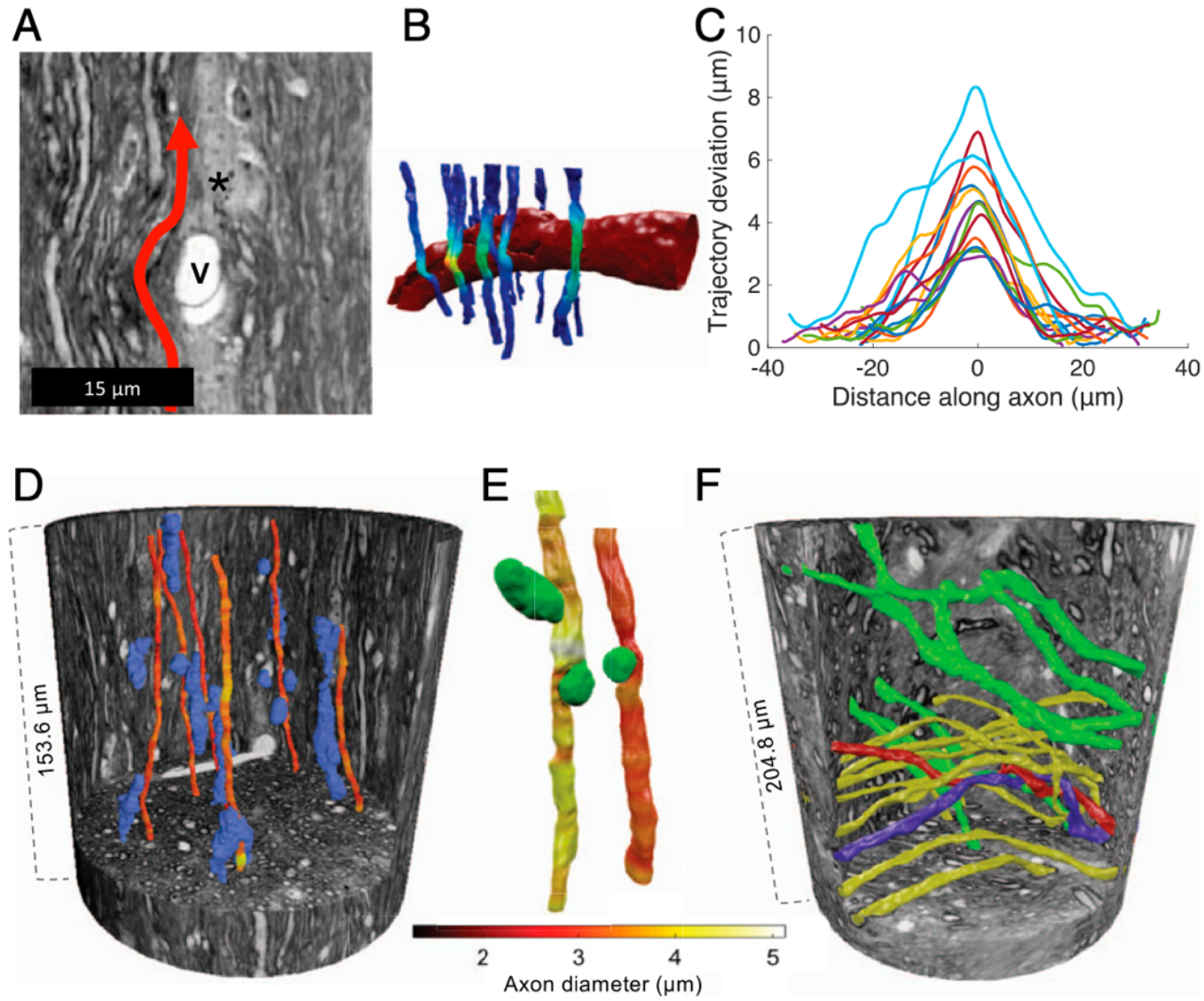

Fig 6. Fig Blood vessels, vacuoles, and crossing axons cause axonal trajectory variations. (A) XNH image looking into a vessel, marked V. Cell nuclei, marked by an asterisk, cluster around the vessel. The vessel significantly impacted the nearby axonal trajectories, depicted by the red arrow. (B) Three-dimensional reconstruction of A. Fifteen segmented axons are colored according to the deviation from their expected linear trajectories (a linear interpolation of the axon centerline above and below the blood vessel). Yellow, strong deviation; dark blue, little/no deviation. (C) Deviation from expected linear trajectory as a function of distance along the axon, centered on the maximum deviation. (D and E) Three-dimensional reconstructions of select cell clusters (blue), vacuoles (green), and axons, whose diameters are given by the color bar, in the XNH volume of the monkey splenium shown in Fig. 3B. The axon trajectories are impacted by the presence of cell clusters, and their diameters and shapes are impacted by neighboring vacuoles. (F) Three-dimensional reconstruction of axons in an XNH volume of a crossing fiber region. Two different projection directions are marked by green and yellow. Two axons, colored red and blue, twist around each other.

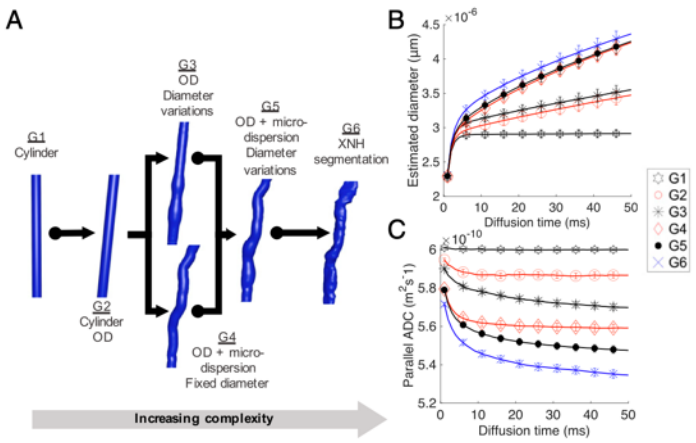

Fig 7. Examining the diffusion properties of different axonal geometries. (A) The morphological features of the XNH-segmented axons in Figs. 3 and 4 are directly mapped to the six different axon classes generated for MC simulations. G1, straight cylinders of diameter corresponding to XNH axon mean diameters; G2, same as G1 plus segmented OD; G3, segmented OD and longitudinal ADD; G4, segmented OD and microdispersion; G5, segmented OD, microdispersion, and longitudinal ADD; and G6, the XNH segmentation. (B) The variation of estimated AD and (C) parallel intra-axonal ADC with diffusion time for geometries G1–G6. Error bars represent the SE, reflecting the spread in diameters/ADCs across the individual axons.

Discussion

By performing high-resolution 3D XNH on intact white matter samples from a monkey brain, we demonstrate the interplay between extra-axonal structures (blood vessels, cells, vacuoles) and the micromorphology of axons. Contrary to Deiters' century- old description of axons as cylinders, we find that AD and tra- jectory vary along the length of the axon, often due to obstacles
in the local microstructural environment. These morphological changes entail that large axons are nonspecific in terms of di- ameter and CV. We thus question the value of precisely mea- suring their diameters and the validity of enforcing cylindrical geometries in axonal structure–function relationships. Further- more, we show that the 3D morphologies of axons may drive previously reported trends in 2D AD distributions and g-ratio distributions. Our results have significant impact for AD deter- mination with 2D techniques and—as we show here—diffusion MRI. We foresee that a thorough morphological characteriza- tion of axons and their structural context will guide the nonin- vasive investigation of axon morphology with diffusion MRI and, consequently, the investigation of brain network function.

For full text, please see https://www.pnas.org/content/117/52/33649.short